

A Biomimetic Polymer Magnetic Nanocarrier Polarizing Tumor-Associated Macrophages for Potentiating Immunotherapy

Lingqiao Liu, Yi Wang, Xing Guo, Jingya Zhao, and Shaobing Zhou*

The progress of antitumor immunotherapy is usually limited by tumor-associated macrophages (TAMs) that account for the highest proportion of immunosuppressive cells in the tumor microenvironment, and the TAMs can also be reversed by modulating the M2-like phenotype. Herein, a biomimetic polymer magnetic nanocarrier is developed with selectively targeting and polarizing TAMs for potentiating immunotherapy of breast cancer. This nanocarrier PLGA-ION-R837@M (PIR@M) is achieved, first, by the fabrication of magnetic polymer nanoparticles (NPs) encapsulating Fe₃O₄ NPs and Toll-like receptor 7 (TLR7) agonist imiquimod (R837) and, second, by the coating of the lipopolysaccharide (LPS)-treated macrophage membranes on the surface of the NPs for targeting TAMs. The intracellular uptake of the PIR@M can greatly polarize TAMs from M2 to antitumor M1 phenotype with the synergy of Fe₃O₄ NPs and R837. The relevant mechanism of the polarization is deeply studied through analyzing the mRNA expression of the signaling pathways. Different from previous reports, the polarization is ascribed to the fact that Fe₃O₄ NPs mainly activate the IRF5 signaling pathway via iron ions instead of the reactive oxygen species-induced NF- κ B signaling pathway. The anticancer effect can be effectively enhanced through potentiating immunotherapy by the polarization of the TAMs in the combination of Fe₃O₄ NPs and R837.

be weakened as a result of the immunosuppressive tumor microenvironment (TME), which is caused by the presence of the immunosuppressive cells and the tumor-associated macrophages (TAMs) account for the most proportion.^[3,4] TAMs can be mainly divided into M1-like cells that inhibit tumor growth and M2-like cells that promote tumor growth.^[5,6] As the main immunosuppressive cells in tumor development, M2 macrophages are dominant in most solid tumors.^[7,8] There are more than 80% of studies revealing that TAMs density correlates with poor patient prognosis.^[9] TAMs can promote the development of malignant tumors, including the invasion and migration of the tumor cells, inhibiting antitumor immune response.^[10,11] Of note, the plastic phenotype of TAM can change in response to the TME into M1 type with antigen-presenting ability and upregulation of the inflammatory cytokines expression. Aiming at the TAMs in the TME,^[12] the nanotechnology-based drug delivery systems can be used to achieve immune adjuvant therapy for cancer,^[13–17] which can be used as an

1. Introduction

Immunotherapy has gradually become a new standard therapy for cancer in recent years, which can stimulate the immune system to recognize and attack tumor cells.^[1] Most immunotherapy strategies aim to produce or release a large number of highly active cytotoxic T lymphocytes (CTLs) to rapidly infiltrate tumor tissues and eliminate tumor cells.^[2] However, the therapeutic effect can

alternative method instead of directly targeting tumor cells. The drug selection and research are ongoing in early clinical trials currently.^[18,19] Increasing evidence indicates that the TAMs-based therapy is potentially effective.^[20]

Because of being potentially beneficial to tumor immunotherapy through polarizing macrophages, more and more attention was focused on how to promote the polarization of TAMs to M1 type. These agents including Fe₃O₄ nanoparticles (NPs),^[21] TLR3 agonist,^[22] TLR7 agonist,^[23] photosensitizer,^[24] etc., have been reported to promote macrophage polarization in tumor tissue and produce certain tumor immunotherapy effect in vivo. Among all of the reports, Fe₃O₄ NPs have received wide attentions. However, the mechanism of Fe₃O₄ NPs-induced macrophages polarization is not clear. Previous study demonstrated that the Fe₃O₄ NPs could produce reactive oxygen species (ROS) and facilitate M1 polarization when co-cultured with macrophages and tumor cells.^[25] Subsequent literatures mentioned that the mechanism of Fe₃O₄ NPs polarized macrophages was based on the Fenton reaction.^[26–29] Although these studies speculate that Fenton reaction promotes TAMs polarization, there is no more in-depth study to prove this process. At the same time, it was also pointed out that the accumulation of iron in the

L. Liu, Dr. Y. Wang
School of Life Science and Engineering
Southwest Jiaotong University
Chengdu 610031, China

Dr. X. Guo, Dr. J. Zhao, Prof. S. Zhou
Key Laboratory of Advanced Technologies of Materials
Ministry of Education
School of Materials Science and Engineering
Southwest Jiaotong University
Chengdu 610031, China
E-mail: shaobingzhou@swjtu.edu.cn

 The ORCID identification number(s) for the author(s) of this article can be found under <https://doi.org/10.1002/sml.202003543>.

DOI: 10.1002/sml.202003543

macrophages could cause the phenotypic switching since Fe_3O_4 NPs could be internalized by macrophages and degraded to iron ions. The high concentration of intracellular iron ions activate the nuclear factor kappa-B (NF- κ B) signaling pathway,^[30] following by the phenotype conversion. In addition to Fe_3O_4 NPs, ionic iron can also polarize macrophages. Fe^{2+} and Fe^{3+} can both induce M1 polarization with the same effect due to iron overload, and increase the expression of IL-1 β , TNF- α , CD86, and inducible nitric oxide synthase (iNOS).^[31] Chelating Fe^{3+} on PDA-PEG NPs was determined to re-educate M2 macrophages.^[32] Fe_3O_4 NPs can induce higher expression levels of CD80/CD87/CD64 than Fe_2O_3 NPs despite the same polarization effect of Fe^{2+} and Fe^{3+} .^[33] In vitro cell signaling pathway experiments have demonstrated that the polarization of Fe_3O_4 NPs is correlated with the interferon-regulatory factor 5 (IRF5) pathway, without the iNOS expression of the NF- κ B pathway induced by ROS, which is different from related reports. Furthermore, Fe_3O_4 NPs could stimulate macrophages to express inflammatory responses by activating the TLR4 signaling pathway on the surface of cell membrane.^[34] Therefore, it is particularly valuable to study whether Fe_3O_4 NPs generate ROS through Fenton reaction to induce TAMs polarization. Furtherly, Fe_3O_4 NPs and other agent that can promote TAMs polarization are combined to obtain a better polarization effect of TAMs. In addition, the membrane of lipopolysaccharide (LPS)-treated macrophages that specifically target TAMs was coated on the NPs to increase the polarization effect of TAMs in vivo.^[35]

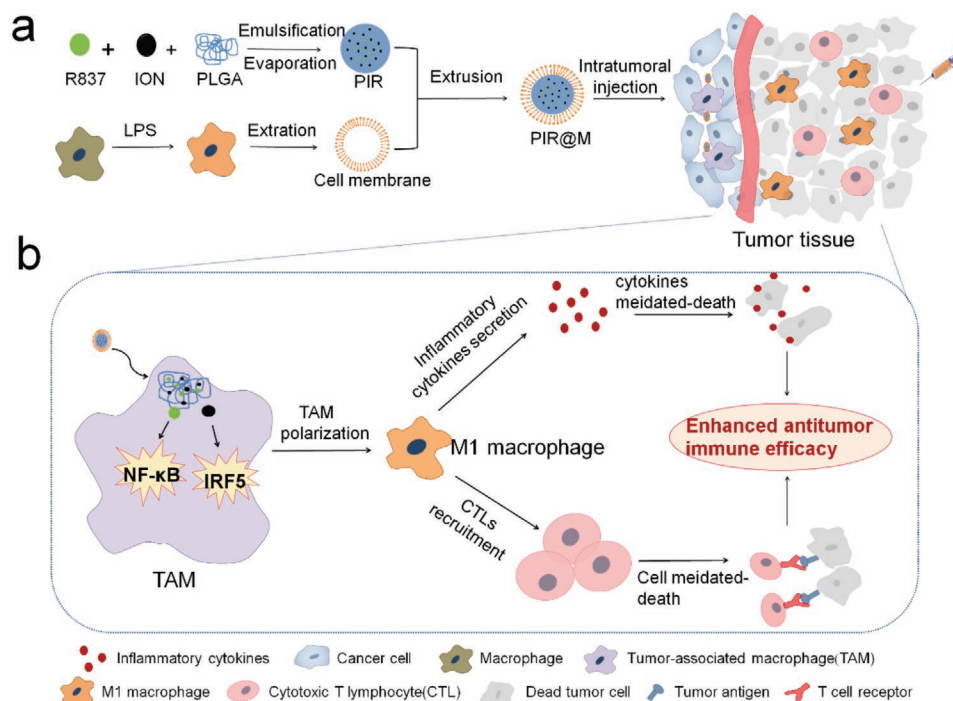
In this study, we developed a cell membrane-coated polymer magnetic nanocarrier with selectively targeting and polarizing

TAMs for potentiating immunotherapy of breast cancer. Poly(lactic-co-glycolic acid) (PLGA) is selected as the matrix of the nanocarriers owing to its excellent biocompatibility and full biodegradation in vivo. This nanocarrier (PLGA-ION-R837@M (PIR@M)) is fabricated as shown in Scheme 1a. First, PLGA-ION-R837 (PIR) NPs loaded with ≈ 13 nm oleic acid-modified Fe_3O_4 NPs (ION) and R837 are fabricated through emulsification and solvent evaporation method. Later, these NPs are coated by M1 macrophage membranes from LPS-treated macrophages by serial extrusions through a 200 nm sized polycarbonate membrane to achieve the resultant PIR@M nanocarriers. With the specific uptake by TAMs for the membrane components, Fe_3O_4 NPs can mainly stimulate the IRF5 signaling pathway while the R837 mainly activates the NF- κ B signaling pathway for enhanced polarization by this synergy effect. The polarization promotes the release of a series of inflammation cytokines, and improves the T-lymphocytes infiltration in tumor tissues. Additionally, the improved phenotype conversion from M2 type to M1 type induced by PIR@M NPs can alleviate the immunosuppression of the TME for immune recovery and apoptosis of tumor cells (Scheme 1b).

2. Results and Discussion

2.1. Preparation and Characterization of the Nanocarriers

To directly observe the encapsulation of Fe_3O_4 NPs, the transmission electron microscopy (TEM) image of PIR@M NPs was



Scheme 1. a) Scheme of the preparation of M1 macrophage cell membrane-coated nanocarriers loaded with Fe_3O_4 NPs and R837 (PIR@M NPs). b) Schematic illustration depicting that the PIR@M NPs polarized the TAMs to M1 phenotype through activating the NF- κ B and IRF5 signaling pathways after intratumoral injection. The polarization toward M1 phenotype increases the secretion of inflammatory cytokines which can directly induce the apoptosis of tumor cells, the inhibition degree of CTLs induced by TAMs can be reduced as well. Enhanced infiltration of the CTLs and the inflammatory factors in tumor tissue could achieve an antitumor immunotherapy effect.

taken without negative staining due to the contrast of the metal iron (Figure 1a). The Fe₃O₄ NPs are spherical and the diameter is measured to be 8.2 ± 0.6 nm (Figure S1 in the Supporting Information), which is in accordance with the result measured by TEM in Figure 1a, and slightly smaller than hydrated particle size shown in Figure S2 in the Supporting Information owing to the evaporation of the solvent. The diameter of the Fe₃O₄ NPs-constituted core in PIR@M NPs is measured to be 110.8 ± 13.8 nm. Moreover, the analysis of the magnetic properties of the nanoparticulate system by vibrating sample magnetometer could also prove the successful encapsulation of Fe₃O₄ NPs since the coercivity is 0 and no hysteresis loop exists (Figure S3, Supporting Information).^[36,37] The TEM image of PIR@M NPs with negative staining was also taken to observe the whole morphology and the membrane structure (Figure 1b). The membrane layer with a size of ≈10 nm in thickness is clearly visible.^[38] The TEM image of PIR@M NPs exhibits a spherical and evenly dispersed morphology with a size of 148.3 ± 7.6 nm, which is similar to the result measured by atomic force microscope (AFM) in Figure S4 in the Supporting Information.

The particle size and zeta potential were also used to investigate the preparation process. As shown in Figure 1c, compared with PIR NPs, the change in particle size and ζ potential of PIR@M NPs characterized by the dynamic light scattering (DLS) further proves the successful modification of membrane components on the NPs. The hydrated particle size of PIR@M NPs is measured to be 166.2 ± 1.8 nm, and the ζ potential is -22.8 ± 0.4 while that of PIR NPs is -19.1 ± 0.1. In addition,

PLGA-R837 (PR) NPs loaded with R837, PLGA-ION (PI) NPs containing Fe₃O₄ NPs, membrane-coated PLGA-R837@M (PR@M) NPs, and PLGA-ION@M (PI@M) NPs were also prepared in the same method for comparison. Due to the coating of the cell membrane, the particle sizes of PR@M and PI@M NPs both increase by ≈20 nm compared to PR and PI NPs (Figure S5, Supporting Information). The membrane protein contents and types were detected by Bradford protein kit and sodium dodecyl sulfate polyacrylamide gel electrophoresis (SDS-PAGE) due to their vital position in cell function. The membrane protein content of PIR@M NPs is 2.62% similar to that of PI@M and PR@M NPs (Figure 1d). There are almost no bands in PIR NPs, indicating no protein components exist. Moreover, the clear protein bands can be seen in cell membrane vesicles (M), indicating that there are plenty of protein components with different molecular weights on the cell membrane. Similarly, the clear bands are also observed in PIR@M NPs, and the protein distribution is the same as the M group, further proving that the PIR NPs are successfully enveloped by the cell membrane (Figure 1e). Due to the presence of membrane components, the released R837 of PIR@M NPs is lower than that of PIR NPs (Figure 1f). The loading contents of Fe₃O₄ NPs and R837 were measured by thermogravimetric analysis (TGA) and UV-visible spectrophotometer (UV-vis), respectively (Figure S6 and Table S1, Supporting Information), and the prepared nanocarriers possess satisfactory loading capacity (LC) and encapsulation efficiency (EE). The LC and EE of Fe₃O₄ NPs are 10.7% and 46.8% while those of R837 are 2.5% and 58.5%, respectively. No significant difference exists among

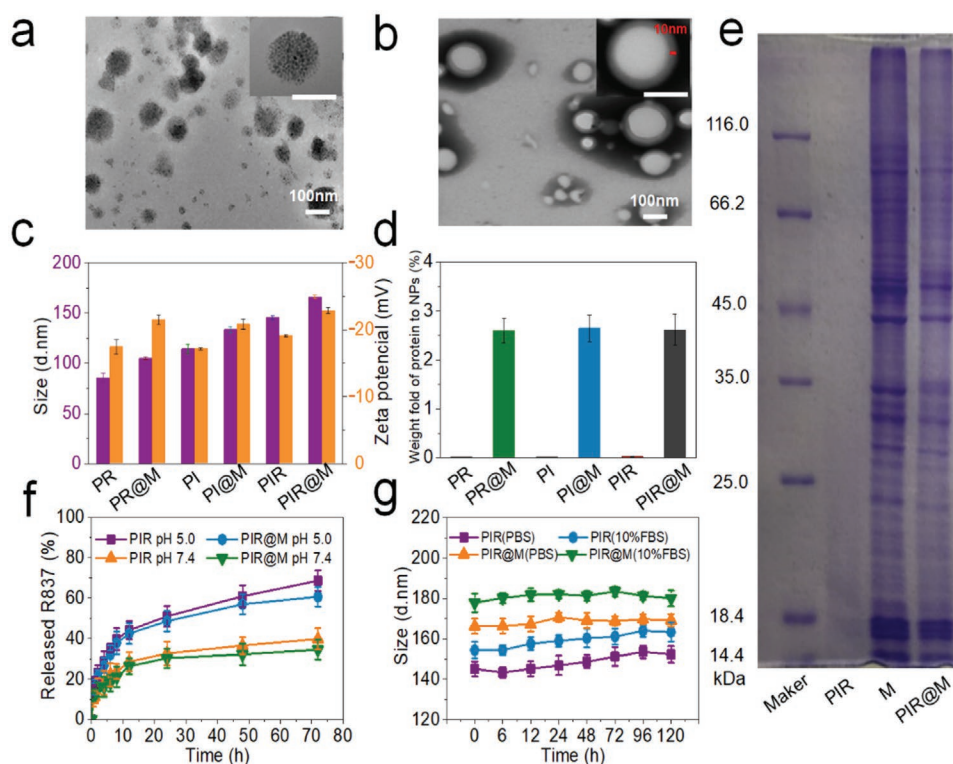


Figure 1. Characterization of nanocarriers. a) The TEM images of PIR@M (without negative staining). b) The TEM image of PIR@M (with negative staining). c) Hydrodynamic sizes and zeta potentials of PR, PR@M, PI, PI@M, PIR, and PIR@M NPs. d) The weight fold of the membrane protein to PR, PR@M, PI, PI@M, PIR, and PIR@M NPs. e) Representative SDS-PAGE protein analysis of PIR NPs, cell membranes (M), and PIR@M NPs. f) The released profiles of R837 in vitro. g) Stability assessment of PIR and PIR@M NPs in PBS and 10% FBS during 120 h.

the particle sizes during 120 h whether dispersed in phosphate buffered saline (PBS) or 10% fetal bovine serum (FBS), exhibiting a good stability (Figure 1g).

2.2. Cytocompatibility Assessment

The toxicity of the blank nanomaterials without R837 against human umbilical vein endothelial cells (HUVEC), 4T1 cells, and mouse peritoneal macrophages was determined by Alamar blue assay and fluorescence microscope (FM). The blank PLGA (P) NPs, cell membrane-coated PLGA@M (P@M) NPs, and cell membrane vesicles (M) were prepared for comparison. The survival rates of HUVEC are above 85% with the intact cell morphology and structure for all of these NPs, indicating a good biocompatibility of the NPs (Figures S7a and S8a, Supporting Information). For 4T1 cells, the cell viability is higher than 85% when treated with the NPs up to $200 \mu\text{g mL}^{-1}$, exhibiting good cell compatibility. The viability of PI@M NPs is 85.3%, which is higher than PI NPs (77.4%) under the concentration of $400 \mu\text{g mL}^{-1}$ owing to the membrane profiles (Figures S7b and S8b, Supporting Information). For macrophages, the survival rates of P, M, and P@M NPs in the range of $400 \mu\text{g mL}^{-1}$ are more than 90%. The viability of PI@M NPs in $400 \mu\text{g mL}^{-1}$ is 75.5%, there is a better biocompatibility of PI@M NPs under the concentration of $200 \mu\text{g mL}^{-1}$ with a cell viability of 86.7%, which can be used as the appropriate concentration for subsequent cell experiments. It is worth noting that the viability of PI NPs is 77.4% in the same concentration condition, indicating the cytocompatibility of PI@M NPs is better than PI NPs due to the coating of membrane components (Figures S7c and S8c, Supporting Information).

2.3. Targeting Ability of NPs

The fluorescent dye coumarin-6 (C6) was utilized to be entrapped in PLGA NPs instead of Fe_3O_4 NPs to obtain

PLGA-C6 (PC) and PLGA-C6@M (PC@M) NPs for intuitive observation. M2 macrophages were incubated with PC and PC@M NPs in different durations. The stronger green fluorescence could be observed with the increased incubation time, revealing the increment of cellular uptake. Therefore, the uptake of NPs by M2 macrophages is time-dependent (Figure 2a). According to the quantification detected by flow cytometry (FCM; Figure 2b,c), the fluorescence intensity of PC@M group is 1.87-fold compared to PC group in 2 h incubation, indicating more uptake of the PC@M as a result of the membrane with M2 macrophages targeting.

To verify whether PC@M NPs could mainly act on M2 macrophages instead of tumor cells, the internalization of NPs by M2 macrophages and 4T1 cells was also determined. As shown in Figure 2d, it is found that the intracellular green fluorescence of PC@M group is higher than that of PC group. There is a significant difference between the uptake of the two types of cells, suggesting that the NPs camouflaged with membranes could target to M2 macrophages (Figure 2e,f).

Moreover, the effect of NPs uptake by tumor cells on tumor cell phenotype such as the expression of TGF- β and PD-L1 was investigated through 4T1 cells shows internalization. As shown in Figure S9 in the Supporting Information, the TGF- β could be secreted by 4T1 cells with the expression level of $648.51 \text{ pg mL}^{-1}$. No significant difference exists among all the groups whether loaded with polarization drugs or coated with membrane, proving that the NPs do not affect the secretion of that cytokines by tumor cells. Similarly, incubation with the nanomaterials does not obviously affect the expression level of PD-L1 as well.

2.4. Investigation on the Polarization Mechanism of Macrophages In Vitro

PI@M NPs were utilized to investigate the polarization mechanism. It was first investigated whether the PI@M NPs can

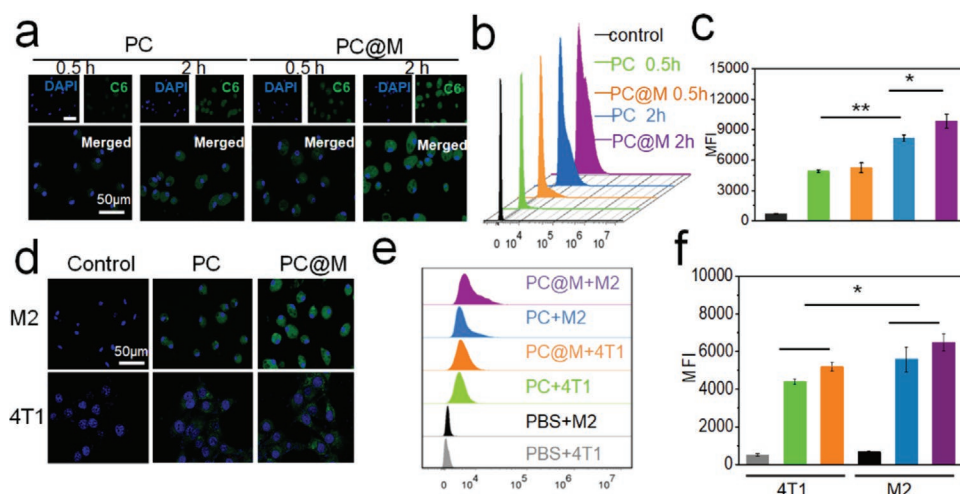


Figure 2. In vitro cellular uptake and targeting ability of NPs. a) Representative fluorescent images of M2 macrophages incubated with PC and PC@M NPs for 0.5 and 2 h. b) FCM analysis of the cellular uptake treated with PC and PC@M NPs for different incubation time. c) Mean fluorescence intensity of the M2 macrophage treated with materials for 0.5 and 2 h. d) Representative fluorescent images of M2 macrophages and 4T1 cells incubated with PC and PC@M NPs for 1 h. e) FCM analysis of the cellular uptake treated with different materials for 1 h. f) Mean fluorescence intensity of the M2 macrophages and 4T1 cells treated with materials for 1 h (* $p < 0.05$, ** $p < 0.01$, *** $p < 0.001$).

stimulate the M2 macrophages to release ROS induced by Fenton reaction.^[25] Indeed, the macrophages are stimulated by PI@M NPs to produce ROS (Figure S10, Supporting Information). The amount of ROS is increased along with the incubation time, probably resulted from the increased substrate of the Fenton reaction.^[39] The maximum concentration of PI@M NPs is considered to be 200 $\mu\text{g mL}^{-1}$ according to the cytocompatibility assessment. Especially, the ROS production of PI@M NPs significantly increases in that concentration, which can be chosen as the experimental condition for the investigation of the polarization.

To verify whether the polarization mainly depends on the ROS pathway, ROS scavenger vitamin C (Vc) was introduced, and the production of ROS after incubation with different materials was investigated. The LPS was added as a positive control, namely, M1 macrophages. M1 macrophages could produce few ROS since weak fluorescence is observed (Figure 3a,b). The groups containing Fe_3O_4 NPs show an ROS fluorescence expression because of the Fenton reaction. ROS could be effectively removed by Vc.^[40] It exhibits a reduced fluorescence intensity, which is 0.69-fold compared to PI@M group under the condition of preincubating with Vc. Next, the effect of nanomaterials loaded with Fe_3O_4 NPs on macrophage phenotypic conversion was explored by labeling M1 macrophages with $\text{F4/80}^+\text{CD80}^+$. As shown in Figure 3c,d, the macrophages could be polarized by PI@M NPs with a positive rate of 74.31%, which is not significantly different from that of the Vc preincubation group. The elimination of ROS may not obviously affect

the polarization function of PI@M NPs on these macrophages, indicating that the way of polarization may not be mainly caused by ROS induced by Fenton reaction. To further examine whether the phenotype conversion was caused by the iron ions, Fe^{2+} and Fe^{3+} were used for comparison, and the production of ROS was detected by the probe and the degree of polarization was measured by FCM as well. Both Fe^{2+} and Fe^{3+} stimulate M2 macrophages to produce a small amount of ROS, but the fluorescence intensity significantly reduced after preincubation with Vc. And the results of FCM show that both Fe^{2+} and Fe^{3+} could moderately stimulate macrophages to M1 phenotype with a positive rate of 20.68% and 21.47%, respectively. However, there is no significant difference in the degree of polarization whether supplemented with Vc beforehand. It is also verified that the way of polarization may mainly pass through Fe^{2+} and Fe^{3+} , rather than ROS produced by Fenton reaction.

On this basis, the internalization of iron by the macrophages after incubating with different nanomaterials was evaluated since the iron played an important role in the phenotype conversion.^[30] The cytoplasm is stained red while the internalized iron is stained blue. In the PI@M group, the blue color in the cells could be clearly observed due to the effective uptake, while the blue area is hardly seen with ionic forms of iron (Figure 3e). Compared with the above FCM results, Fe^{2+} and Fe^{3+} only moderately induce the conversion while PI@M NPs have a higher degree of M1 phenotype polarization. Thus, the intracellular Fe^{2+} and Fe^{3+} might be a vital factor in the polarization.^[33]

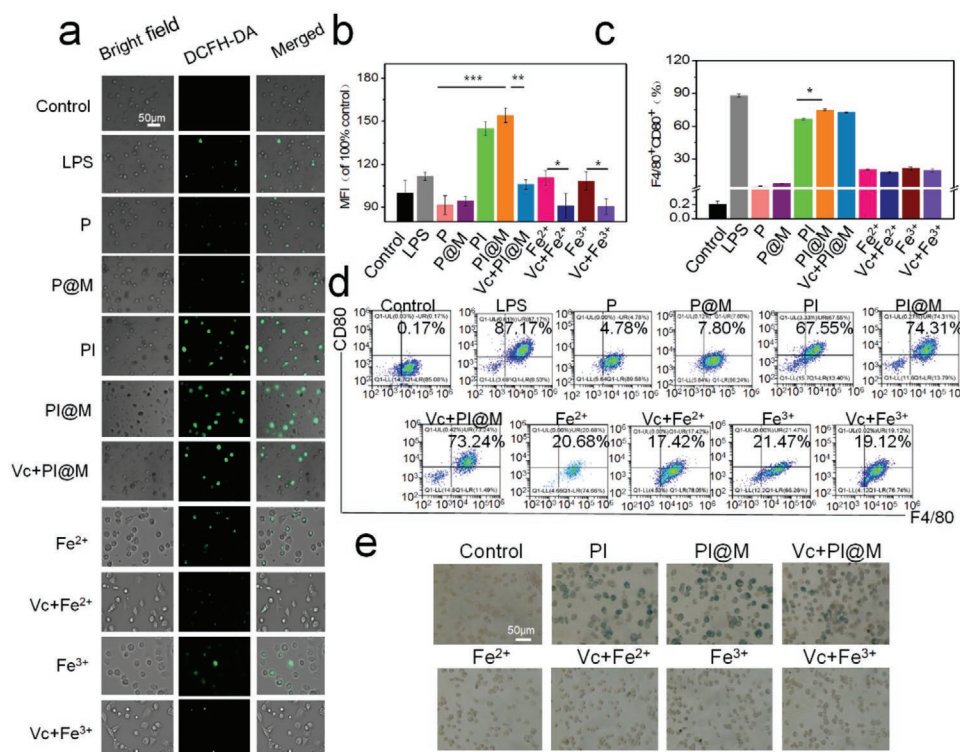


Figure 3. The polarization mechanism of macrophages in vitro. a) Representative bright field and fluorescence images of M2 macrophages incubated with nanomaterials, the generated ROS were stained with ROS probe (green). b) Mean fluorescence intensity of ROS after incubation. c) Percentage of $\text{F4/80}^+\text{CD80}^+$ cells. d) Representative flow cytometry plots of macrophages incubated with nanomaterials. e) Prussian blue staining of macrophages treated with nanomaterials ($*p < 0.05$, $**p < 0.01$, $***p < 0.001$).

2.5. Investigation on the Co-Polarization Effect

As that the mechanism of Fe₃O₄ NPs polarizing macrophages may not mainly dependent on the ROS that could induce NF- κ B signaling pathway,^[41] another polarization agent R837 that could activate the NF- κ B signaling pathway via TLR7 was introduced in the combination with Fe₃O₄ NPs to achieve an enhanced polarization effect.^[42] Then, the production of ROS induced by Fe₃O₄ NPs and R837 after incubated with macrophages was detected. The FM images of ROS probe are shown in **Figure 4a**, the PI@M NPs could stimulate the M2 macrophages to generate ROS, while PR@M group only produces a quite fewer of ROS. Therefore, the fluorescence intensity of PIR@M group is not much different from that of the PI@M group. However, it is reduced to 0.66-fold when supplemented with Vc (Figure 4b). Next, the polarization degree of macrophages was assessed. As shown in Figure 4c,d, the positive rate of the PR@M group is 78.04%, which is higher than that of PI@M group. The positive rate of PIR@M group reaches to 85.17%. After the preincubation with Vc, the result is not significantly different from the PIR@M group, further indicating that the ROS pathway may not be the main pathway of the macrophages polarization by Fe₃O₄ NPs. Of note, there is a satisfactory co-polarization effect in the combination of Fe₃O₄ NPs and R837.

2.6. Transwell Assays

Inspired by the above results, the hypothesis that PIR@M NPs would induce a stronger tumor killing effect based on the better polarization ability than single polarization agent was assessed.

Transwell co-culture chambers were used to simulate TEM, and the killing effect on tumor cells after polarizing macrophages with different nanomaterials was examined. As depicted in Figure 4e, 4T1 cells were seeded on the lower layer and macrophages were seeded on the 0.4 μ m sized microporous membrane of chamber at the ratio of 1: 3. The viability of lower tumor cells was evaluated by Alamar blue assay. In Figure 4f, the PI@M group is nearly nontoxic to 4T1 cells whether preincubated with Vc. The cell survival rates of those two groups are 88.1% and 83.9%, respectively. The PR@M group has a stronger killing effect with a survival rate of 55.3%. However, none achieves the half suppression effect. It has been concluded that combining Fe₃O₄ NPs with R837 could effectively polarize macrophages. As expected, the PIR@M group exerts a synergistic killing effect with the cell viability of 27.3%. Of note, the cell survival rate of the PIR group is 64.2%, which was much higher than that of the PIR@M group, proving that a better polarization and tumor killing effect are achieved owing to the TAMs targeting property and M1 phenotype-inducing property of PIR@M nanocarriers. Thus, PIR@M NPs could effectively inhibit 4T1 cells growth, indicating the feasibility of antitumor experiments in vivo.

2.7. In Vivo Macrophages Polarization and Evaluation of Antitumor Immunity

Considering the promising polarization and killing effect of the PIR@M NPs in vitro, in vivo assessment was further performed. Specific pathogen-free (SPF) female BALB/c mice were used to establish orthotopic breast cancer models by

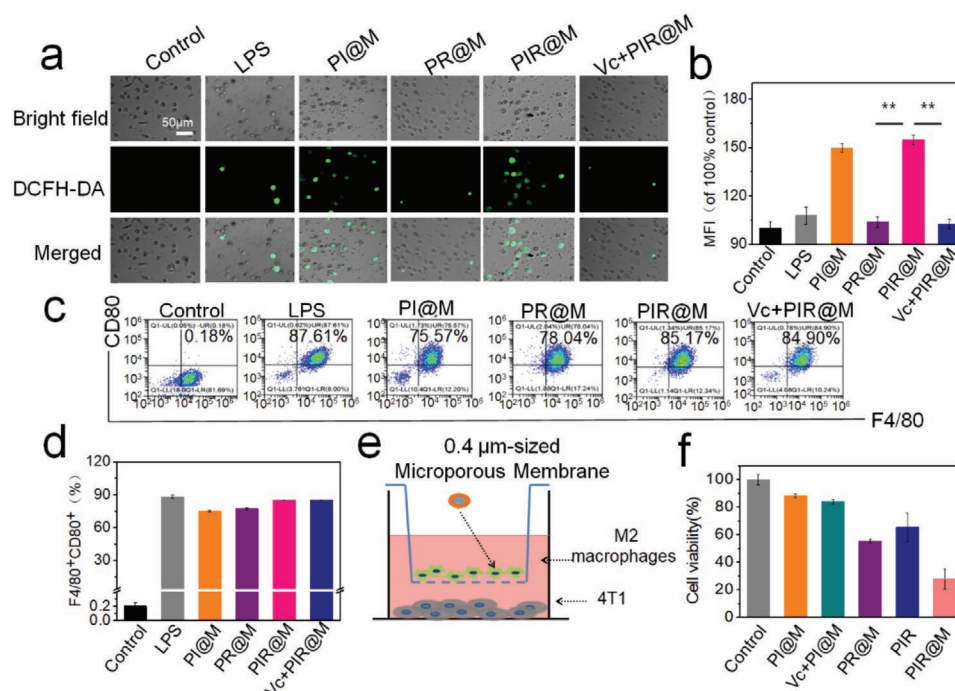


Figure 4. The co-polarization effect. a) Representative bright field and fluorescence images of M2 macrophages incubated with nanomaterials, the generated ROS were stained with ROS probe (green). b) Mean fluorescence intensity of ROS after incubation. c) Representative flow cytometry plots of macrophages incubated with nanomaterials. d) Percentage of F4/80⁺CD80⁺ cells. e) Schematic of the co-culture system. f) Cell viability assessment of the lower 4T1 cells in the co-culture system (**p* < 0.05, ***p* < 0.01, ****p* < 0.001).

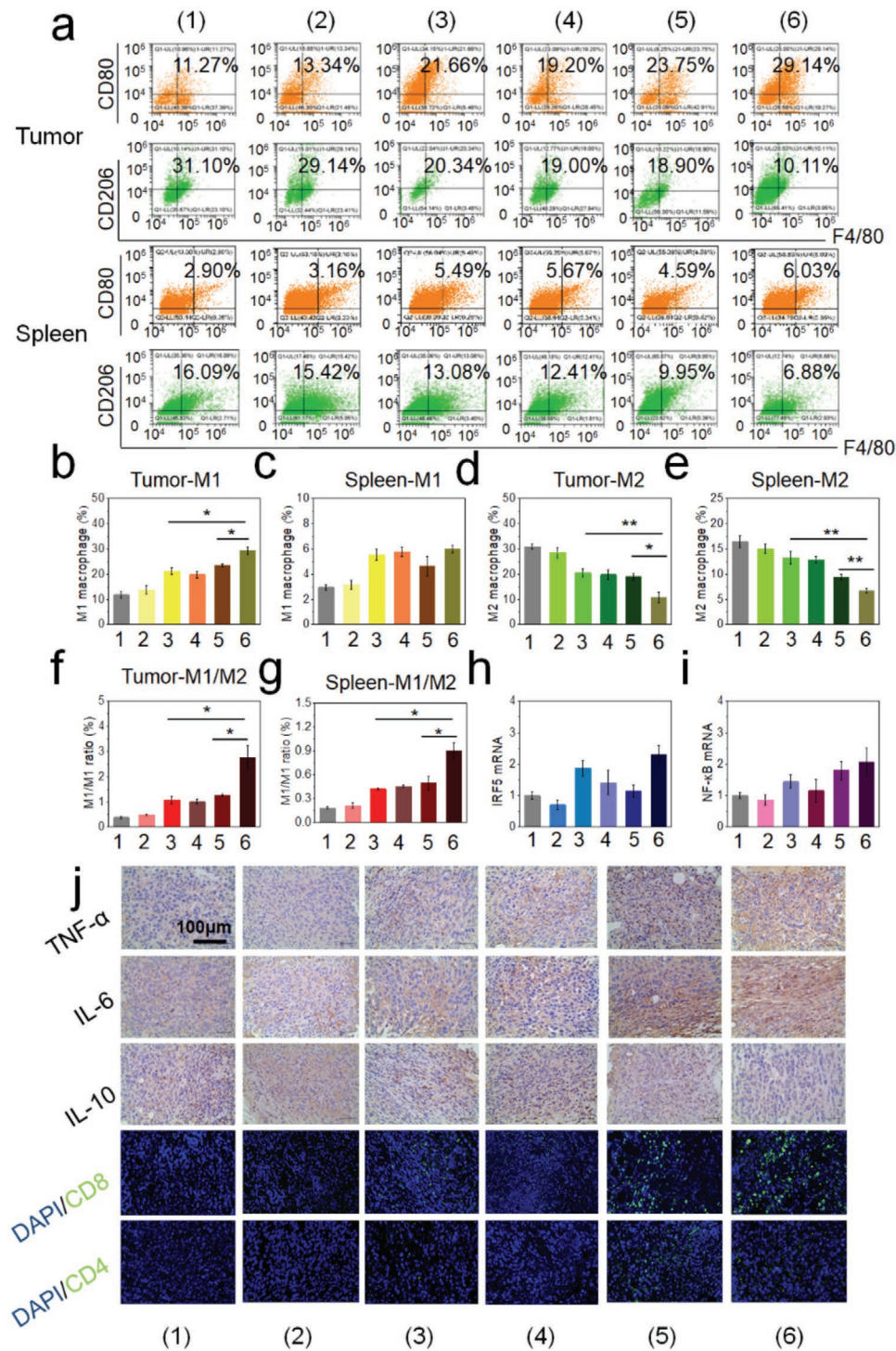


Figure 5. In vivo macrophage polarization and antitumor immunity. a) Proportion of M1 macrophages (labeled with F4/80⁺CD80⁺) and M2 macrophages (labeled with F4/80⁺CD206⁺) in tumor tissue and spleen. Percentage of F4/80⁺CD80⁺ cells in b) tumor and c) spleen, respectively. Percentage of F4/80⁺CD206⁺ cells in d) tumor and e) spleen. The ratio of M1/M2 subtype in f) tumor and g) spleen. The relative mRNA expression of h) IRF5 and i) NF-κB signaling pathway. j) Immunohistochemical staining for TNF-α, IL-6, and IL-10 cytokines of tumor sections after treatments and immunofluorescence staining images for cytotoxic CD8⁺ (green) and helper CD4⁺ T-lymphocytes (green) of tumor sections after treatments [(1), (2), (3), (4), (5), and (6) represent saline, P@M, PI@M, Vc+PI@M, PR@M, and PIR@M groups, respectively] (**p* < 0.05, ***p* < 0.01, ****p* < 0.001).

subcutaneously inoculating 4T1 cells into the mouse mammary fat pads. To enable the NPs to be enriched in the tumor sites, the mice were received intratumoral injections of the

NPs every 2 days. The classifications of macrophages in tumor tissues and spleens are shown in **Figure 5a**. In tumor tissues, TAMs could be effectively polarized by PI@M NPs

loaded with Fe₃O₄ NPs, and the percentage of M1 macrophages increases from 11.27% to 21.66%, which of M2 macrophages decreases from 31.10% to 20.34%, leading to an increase of the ratio of M1/M2 from 0.36 to 1.06. The M1/M2 ratio of the PR@M group loaded with R837 was 1.26. For the PIR@M group, M1 macrophages account for 29.14%, M2 macrophages account for 10.11%, and the M1/M2 ratio increases to 2.88. The polarization effect is greatly improved when Fe₃O₄ NPs are in association with R837. A similar result is observed in spleen tissue, which is the largest immune organ in vivo, and the M1/M2 ratio of PIR@M group increases from 0.18 to 0.88, proving that PIR@M NPs have a satisfactory phenotypic conversion function (Figure 5b–g).

The mRNA expression of IRF5 and NF- κ B signaling pathways related to macrophage polarization in tumor tissues was investigated to further assess the activation level and the polarization mechanism. As shown in Figure 5h,i, the IRF5 signaling pathway is effectively activated by PI@M NPs and the relative expression is 1.30-fold that of the NF- κ B, indicating that the polarization induced by Fe₃O₄ NPs is mainly depended on the IRF5 signaling. Because the IRF5 signaling pathway can be activated by intracellular Fe²⁺ and Fe³⁺, which is consistent with the result of in vitro cell experiments. Different from PR@M NPs, where the NF- κ B pathway is the main activated pathway, the relative expression of NF- κ B gene increases to 1.57 times compared with that of the IRF5 gene in PR@M group. As expected, the high expression of IRF5 gene and NF- κ B gene in PIR@M NPs leads to the best polarization effect among all groups.

The phenotypic conversion would effectively facilitate the apoptosis of tumor. On the one hand, the polarization of TAMs to M1 type could promote the release of inflammatory cytokines such as TNF- α , which could directly kill tumor cells through the death receptor signaling pathway.^[43] Compared with others, PIR@M NPs present more positive regions of the inflammatory cytokines (Figure 5j), which is consistent with the FCM results. The release of anti-inflammatory cytokine IL-10 is also reduced after polarization. Namely, the M1 relative makers (TNF- α and IL-6) of the PIR@M group are obviously enhanced, while the M2 relative maker (IL-10) expresses less. On the other hand, the inhibition of CLTs by TAMs could be reduced owing to the phenotypic switching to M1 type, the infiltration of T-lymphocytes in tumor tissues is promoted as well. Subsequently, the infiltration of T-lymphocytes was detected by immunofluorescence (IF) staining. Both the green fluorescence of cytotoxic CD8⁺ and helper CD4⁺ T-lymphocytes in PIR@M group are obviously increased in comparison with others, revealing the best polarization effect among all groups.

2.8. In Vivo Tumor Inhibition Studies

The treatment was started and recorded as day 0 when the tumor burden reached 50 mm³. The images of mice at day 0 and day 21 are displayed in Figure 6a. The images of tumor tissues harvested from different groups on day 21 (Figure 6b) and the tumor volume growth curves (Figure 6c) indicate that PI@M, Vc + PI@M, PR@M, and PIR@M groups show tumor suppressive outcome. Compared with the 21 day tumor volume

of the saline group (increased \approx 9.9-fold), the volume of PI@M group loaded with Fe₃O₄ NPs and Vc + PI@M group increases approximately seven times, exhibiting a mild antitumor effect with the tumor growth inhibition (TGI) of \approx 30% (Figure 6d). PR@M group containing R837 shows a better tumor inhibition effect, the volume improved \approx 3.7 times with the tumor inhibition rate of 62.5%. As expected, the best tumor inhibition effect is achieved from the PIR@M group, and the tumor inhibition rate reaches 72.5% in the combination of Fe₃O₄ NPs and R837. Furthermore, there is no significant difference in body weights among groups, indicating that the NPs almost have no side effect to body (Figure 6e).

Subsequently, histochemical staining was assessed to further evaluate the therapeutic effect and safety (Figure 6f). The hematoxylin and eosin (H&E) staining of tumors indicates that all the groups exhibit different degrees of cell necrosis except the saline and P@M group, and the PIR@M group shows the best antitumor effect. In addition, the terminal deoxynucleotidyl transferase dUTP nick end labeling (TUNEL) assays show that the area of apoptosis of the PIR@M group is the largest among all groups, which is consistent with the stronger antitumor effect. And the labeled area of Ki67 assays is smaller than other groups, indicating the weak proliferation levels of tumor cells. The results of the PIR@M group are significantly different from those of the PI@M and PR@M groups, demonstrating that an enhanced therapeutic effect is achieved (Figure S11, Supporting Information). The H&E staining of the vital organs (heart, liver, spleen, lung, and kidney) harvested from mice shows no obvious histopathologic changes in PIR@M group in comparison with the saline group (Figure S12, Supporting Information), suggesting that the nanomaterials are biocompatible without systemic toxicity. The same conclusion could be obtained from the hematology tests, where the blood parameters are within a normal range (Figure S13, Supporting Information). In a word, the anticancer effect of PIR@M NPs can be effectively enhanced through potentiating immunotherapy by a polarization of the TAMs in the combination of Fe₃O₄ NPs and R837.

3. Conclusion

In summary, a biomimetic polymer magnetic nanocarrier is successfully developed, which possesses a great capacity of potentiating immunotherapy of breast cancer through selectively targeting and polarizing TAMs. A polarization effect with the M1/M2 ratio of 2.88 is achieved in tumor tissue by the combination of Fe₃O₄ NPs and R837 in this nanocarrier. The polarization mechanism was deeply investigated through analyzing the mRNA expression and the result indicates that Fe₃O₄ NPs mainly activate the IRF5 signaling pathway with iron ions instead of ROS-induced NF- κ B signaling pathway while R837 activates the NF- κ B pathway. As a result, the upregulation of both the pro-inflammatory cytokines such as TNF- α and the infiltration of T-lymphocytes in tumor tissues are promoted. Finally, an enhanced anticancer effect is obtained by the improved immunotherapy. Therefore, this work provides a new strategy by remodeling tumor microenvironment to potentiate immunotherapy for cancer treatment.

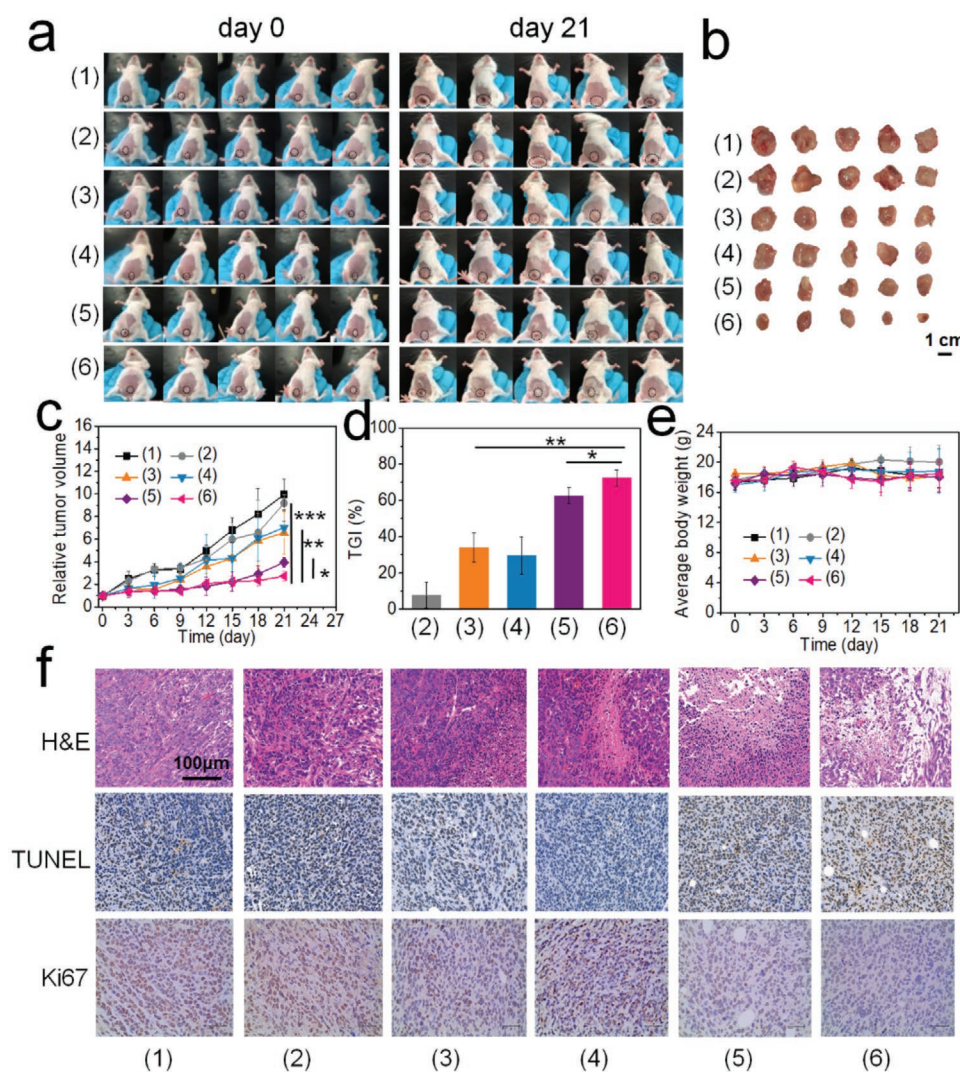


Figure 6. In vivo antitumor effect. a) The images of tumor-bearing mice at day 0 and day 21. b) Representative images of tumor tissues isolated from different therapy groups. c) The relative tumor volume growth curves of tumor-bearing mice during treatments. d) TGI of tumor-bearing mice with different treatments. e) Average body weight curves during 21 day treatment. f) H&E, TUNEL, and Ki67 staining images of tumor tissue harvested from different therapy groups [(1), (2), (3), (4), (5), and (6) represent saline, P@M, PI@M, Vc+PI@M, PR@M, and PIR@M groups, respectively] (* $p < 0.05$, ** $p < 0.01$, *** $p < 0.001$).

4. Experimental Section

Materials: Ferric trichloride hexahydrate ($\text{FeCl}_3 \cdot 6\text{H}_2\text{O}$), ferrous chloride tetrahydrate ($\text{FeCl}_2 \cdot 4\text{H}_2\text{O}$), ammonium hydroxide ($\text{NH}_3 \cdot \text{H}_2\text{O}$), and oleic acid were purchased from Aladdin, China. Dimethyl sulfoxide (DMSO), tetrahydrofuran (THF), and acetone were purchased from Chengdu KeLong Chemical Reagent Company, China. PLGA ($M_n = 8000$) was purchased from Jinan Daigang life technologies, China. Imiquimod (R837) was purchased from Adamas-beta, China. 2',7'-Dichlorodihydrofluorescein diacetate (DCFH-DA), Bradford reagent, and LPS were purchased from Sigma Aldrich, USA. C6 was purchased from TCI, Japan. Recombinant murine IL-4 was purchased from Peprotech, USA. Anti-F4/80 FITC (clone: BM8), anti-CD80 APC (clone: 16-10A1), anti-CD206 APC (clone: MR6F3) were purchased from Thermo Fisher Scientific, USA. 70 μm nylon cell strainer and 0.4 μm sized Transwell plates were purchased from Corning, USA. Enzyme-linked immunosorbent assay (ELISA) kits (TGF- β and PD-L1) were purchased from MEIMIAN, China.

Cell Lines and Culture Conditions: Fresh mouse peritoneal macrophages, RAW264.7 and the 4T1 murine breast cancer cells were all cultured in

Dulbecco's modified Eagle's medium (DMEM) medium (Hyclone) containing 10% FBS, with 5% CO_2 in an incubator at 37 $^\circ\text{C}$ (Thermo Fisher Scientific, USA). The fresh mouse peritoneal macrophages were harvested according to previously reported method.^[44] The mouse was intraperitoneal injected with 5% sterilized starch broth for three times before sacrificed and immersed in 75% ethanol to sterilize. Then the body was intraperitoneal injected with 5 mL DMEM medium, followed by gently rubbing the abdomen and withdrawing the medium, repeated three times. The fresh peritoneal macrophages contained in the withdrawn medium could be cultured in incubator. Standard M1 and M2 macrophage was acquired from fresh mouse peritoneal macrophages supplemented with 100 ng mL^{-1} LPS (Sigma-Aldrich, USA) and 40 ng mL^{-1} IL-4 (Peprotech, USA) for 24 h, respectively.

Animals: SPF female BALB/c mice (5–6 weeks, 18 ± 2 g) were feed at the Animal Experimental Center of Sichuan University (China). All animal procedures were conducted with approval under the rules and regulations of the animal care and use committee of Sichuan University.

Synthesis of ION and Development of the Nanocarriers: ION was prepared as the previously reported method.^[45,46] Briefly, $\text{FeCl}_3 \cdot 6\text{H}_2\text{O}$

(2 mmol) was completely dissolved in RO water with mechanical stirring at 50 °C, followed by adding FeCl₂·4H₂O (1 mmol). NH₃·H₂O (40 mL) was added at a rate of three drops per second. After that, the reaction temperature was adjusted to 80 °C, and the oleic acid (3 mmol) was added to continue the reaction for 1 h. The reaction solution was cooled at 4 °C, washed with saturated brine, and then dispersed in THF. As for the drug-loaded NPs, PLGA and ION (PLGA:ION = 10:2 in molar ratio) were dissolved in THF and acetone, respectively. The mixture was dropped into RO water with mechanical stirring to obtain the PLGA-ION (PI) NPs solution. Similarly, PLGA, ION, and R837 (PLGA:ION:R837 = 10:2:1 in molar ratio) were dissolved in THF, DMSO, and acetone, respectively. The mixture was dropped into RO water with mechanical stirring and put into dialysis bags (MWCO = 1000 Da) for 3 days to obtain the PLGA-ION-R837 (PIR) NPs solution. The PLGA (P) and PLGA-R837 (PR) NPs were prepared with the same method.

Preparation of Cell Membrane-Coated Nanocarriers: The cell membrane-coated PLGA-ION@M (PI@M) NPs were prepared as follows: PI NPs were prepared through solvent evaporation, and then deriving the M1 macrophage membranes from LPS-treated macrophages, the M1 macrophages were obtained according to the methods reported.^[35] LPS-treated RAW264.7 were digested by 2 × 10⁻³ M ethylenediaminetetraacetic acid and resuspended in RO water. The mixture was sonicated several times, followed by adding 0.25 M sucrose solution immediately and centrifuging to collect membranes. Cell membrane fragments were obtained by repeated freeze–thaw cycles. Membranes were coated on PLGA NPs core by serial extrusions through a 200 nm sized polycarbonate membrane (Avanti, USA) to prepare the PI@M NPs. The PLGA@M (P@M), PLGA-R837@M (PR@M), and PLGA-ION-R837@M (PIR@M) NPs were prepared in the same method.

Characterization of Nanocarriers: The morphology of the ION was detected by TEM (TECNAI G2 F20, FEI), and the morphology and structure of the PIR@M nanocarriers were detected by TEM (TECNAI G2 F20, FEI) and AFM (CSPM5000). The drug-loading content (LC) and encapsulation efficiency (EE) of ION and R837 were examined by TGA (Netzsch STA 449C, Bavaria) and UV-vis (UV-2550, Shimadzu), respectively. According to the standard absorbance curve, the concentration of R837 was calculated by the absorbance at 318 nm, as well as the count of in vitro R837 release. The decoration of membranes on the NPs was determined by the particle sizes and zeta-potentials obtained from DLS (Nano-ZS90, MALVERN). In addition, surface proteins on the NPs were further characterized by an SDS-PAGE electrophoresis assay. The Bradford Kit was used to determine the content of membrane proteins on the NPs.

Cytocompatibility Assessments: Alamar blue assay and FM (Zeiss Axio Observer) were utilized to determine the cytocompatibility of the NPs against HUVEC, 4T1 cells, and mouse peritoneal macrophages. Cells were seeded in 48-well plates at a number of 2 × 10⁴ cells per well and cultured for 24 h. Different concentrations of materials were added into the medium and cultured for another 24 h. The medium was replaced by the Alamar blue solution and incubated at 37 °C for 3 h in dark. Finally, the absorbance at 570 nm was measured by a microplate reader to analyze the survival. Furthermore, calcein (2 × 10⁻³ M) and propidium iodide (4 × 10⁻³ M) were used to stain with live and death cells for intuitively observing. After the culture of cells with materials, the fluorescent dye was added into the well and incubated with cells for 15 min, and visualized by FM.

Targeting Ability of NPs: The fluorescent dye C6 was entrapped in PLGA NPs to obtain PLGA-C6 (PC) and PLGA-C6@M (PC@M) NPs. M2 macrophages were seeded with a density of 5 × 10⁵ cells into the confocal dishes. PC and PC@M NPs were added into the dishes, respectively, and incubated with the cells at different time (0.5 and 2 h). After incubation, the cells were fixed with 2.5% glutaraldehyde, stained with DAPI (4',6-diamidino-2-phenylindole) for 10 min, and observed the fluorescence of C6 with FM. The excitation and emission wavelengths of C6 were 466 and 504 nm, respectively. FCM (CytoFLEX, Beckman Coulter) was then used to quantitatively analyze the infiltration of NPs into cells. M2 macrophages were seeded into 12-well plates at a density of 1 × 10⁶ cells per well. PC and PC@M were added

and incubated with the cells. The fluorescence intensity in the cells was examined by FCM.

Subsequently, M2 macrophages and 4T1 cells were, respectively, seeded into the confocal dishes, PC and PC@M were added and incubated with the cells for 1 h. The cells were fixed and stained with DAPI, observed by FM. FCM was also used for quantitative analysis.

ELISA Assay: 4T1 cells were seeded in 6-well plates with a density of 30 × 10⁴ cells per well. After 24 h, P, P@M, PIR, PIR@M were added at the same concentration of 200 μg mL⁻¹ and co-cultured for 24 h. The culture medium was collected and the large particles were removed by centrifuging. The samples were tested in accordance with the instruction of TGF-β detection kit. For the detection of the PD-L1 expression, the cells were collected by centrifuging and resuspended in PBS. And the supernatant was collected by centrifuging after repeated freezing and thawing for three times. The samples were tested in accordance with the instruction of PD-L1 detection kit.

Intracellular ROS Detection: M2 macrophages were seeded in 96-well plates with a density of 5 × 10⁴ cells per well. After 24 h, different concentrations of PI@M NPs (converted to 0, 2.5, 5, 10, 15, 20 μg mL⁻¹ ION) were added in order and, respectively, incubated for 1, 3, 6, and 9 h. Then the culture medium was replaced by DCFH-DA (1 × 10⁻⁵ M) and incubated for 20 min. The ROS production in the cells was visualized by FM. Then a microplate reader was used to quantify the production of ROS. After the adding of DCFH-DA for 20 min, the fluorescence of DCF could be directly detected by a microplate reader. The excitation and emission wavelengths of DCF were 488 and 525 nm, respectively. The results of the experimental group were calculated by comparison with the control group, namely, the relative fluorescence intensity of ROS.

In Vitro Macrophages Polarization: Macrophages were inoculated in 12-well plates at a density of 1 × 10⁶ cells in well. 24 h later, the medium was removed, replaced with different materials, and the Vc-containing (0.5 × 10⁻³ M) groups were preincubated for 3 h. And the cells were collected by centrifugation, supplemented with anti-F4/80 FITC (clone: BM8) and anti-CD80 APC (clone: 16-10A1) under the recommended dosages, and incubated at 4 °C for 30 min in dark. Finally, cells were resuspended in PBS for FCM analysis.

Prussian Blue Staining: M2 Macrophages were inoculated in 48-well plates at a density of 1 × 10⁵ cells, PI, PI@M, FeCl₂, and FeCl₃ were added at the same ION concentration of 50 μg mL⁻¹. 2.5% glutaraldehyde was used to fix the cells for 30 min, and treated with 1 mL fresh Perls solution (2% hydrochloric acid:2% potassium ferrocyanide = 1:1, v/v) for 30 min. The cells were washed with PBS for three times and stained with 0.5% neutral red for 5 min. Finally, the bright field images were collected from optical microscope.

Transwell Assays: M2 macrophages and 4T1 cells were, respectively, inoculated into 24-well plates and upper Transwell chambers at a ratio of 3:1 to simulate TME for 24 h. PI@M, PR@M, PIR, and PIR@M (20 μg mL⁻¹ ION) were added and co-cultured for 48 h. The chambers were removed and Alamar blue assay was used to calculate the viability of lower 4T1 cells.

In Vivo Tumor Inhibition Studies: SPF female BALB/c mice were received subcutaneously inoculated 1.0 × 10⁶ 4T1 cells resuspended in 100 μL serum-free DMED medium per mouse into the mammary fat pads. When the tumor volume reached 50 mm³ after 10 days, the mice were randomly divided into six groups (n = 5). Then the tumor-bearing mice were intratumoral injected by 1) saline, 2) P@M, 3) PI@M, 4) Vc+PI@M, 5) PR@M, and 6) PIR@M on day 0, 2, 4, and 6. The body weight and tumor volume were measured every 3 days. The equal dosages of ION and R837 were 12 and 3 mg kg⁻¹, respectively. The tumor volume was calculated as follows: $V = ab^2 / 2$, where V represents the tumor volume, a and b represent the length and the width of the tumor, respectively.

In Vivo Macrophage Polarization: Tumor-bearing mice were sacrificed on day 9, the tumor tissues and spleen tissues from each group were collected for FCM analysis and reverse transcription polymerase chain reaction (RT-PCR) assay. As for FCM analysis, the tumors and spleens were soaked in 4 °C PBS and ground through a sieve. Red blood cell lysate was added for 3 min at room temperature. For the labeling of M1 phenotype macrophages, cells were supplemented with anti-F4/80 (FITC)

and anti-CD80 (APC) and incubated at 4 °C for 30 min, then detected by FCM. For the labeling of M2 phenotype macrophages, cell activation cocktail (Bio Legend) was first added into cell suspension to stimulate the cells for 4 h, the anti-F4/80 (FITC) was added to incubate for 30 min at 4 °C. 500 µL fixation buffer (Bio Legend) was added per tube. After 20 min incubation at room temperature, 1 mL of Intracellular staining permeabilization wash buffer (Bio Legend) was added to resuspend each cell pellet. Finally, cells were supplemented with anti-CD206 (APC) and incubated at 4 °C for 30 min before determined by FCM.

RT-PCR Assays: To compare the signaling pathway of macrophage polarization, associated mRNA expressions were detected. The tumor tissues removed from the euthanized mice on day 9 were utilized for RNA separation and extraction. RT-PCR experiments were performed according to the primers IRF5 and NF-κB designed and synthesized by Shanghai Shengong Co., Ltd. The Ct (Cycle threshold) value of each test sample was analyzed by Thermo Scientific PikoReal software.

In Vivo Evaluation of Antitumor Immunity: Immunohistochemistry staining and immunofluorescence staining were performed to evaluate the antitumor immunity of each therapy group. M1 macrophage relative cytokines (TNF-α, IL-6) and M2 macrophage relative cytokine (IL-10) were investigated by immunohistochemistry staining, the slices were observed by FM. CD4⁺ and CD8⁺ T cells were investigated by immunofluorescence staining, the slices were observed by confocal laser scanning microscopy.

Histological Analysis and Hematology Tests: On the end day of the treatment, mice were euthanized. The heart, liver, spleen, lung, kidney, and tumor were removed, then fixed, and embedded. The tissues were sliced into 4 µm sections and stained with H&E, while tumor tissues were stained with H&E, Ki67, and TUNEL. The images were collected from the optical microscope. The blood samples from orbit collected by saline and PIR@M group were used for hematology tests.

Statistical Analysis: The data measured in the experiments were expressed as mean ± standard deviation, and a single factor analysis of variance (ANOVA) analysis was performed to compare the significant differences between the data. **p* < 0.05, ***p* < 0.01, and ****p* < 0.001 were used to indicate the significance of the difference.

Supporting Information

Supporting Information is available from the Wiley Online Library or from the author.

Acknowledgements

L.L. and Y.W. contributed equally to this work. This work was partially supported by the China National Funds for Distinguished Young Scientists (51725303) and the National Natural Science Foundation of China (21574105, 81701831). The authors thank the Analysis and Testing Center of Southwest Jiaotong University.

Conflict of Interest

The authors declare no conflict of interest.

Keywords

immunotherapy, nanoparticles, polarization, reactive oxygen species, tumor-associated macrophages

Received: June 9, 2020

Revised: July 7, 2020

Published online: August 18, 2020

- [1] S. T. Koshy, D. J. Mooney, *Curr. Opin. Biotechnol.* **2016**, *40*, 1.
- [2] L. Zitvogel, L. Apetoh, F. Ghiringhelli, G. Kroemer, *Nat. Rev. Immunol.* **2008**, *8*, 59.
- [3] S. H. van der Burg, R. Arens, F. Ossendorp, T. van Hall, C. J. M. Melief, *Nat. Rev. Cancer* **2016**, *16*, 219.
- [4] K. M. Mahoney, P. D. Rennert, G. J. Freeman, *Nat. Rev. Drug Discovery* **2015**, *14*, 561.
- [5] B. Z. Qian, J. W. Pollard, *Cell* **2010**, *141*, 39.
- [6] P. Pathria, T. L. Louis, J. A. Varner, *Trends Immunol.* **2019**, *40*, 310.
- [7] V. Bronte, P. J. Murray, *Nat. Med.* **2015**, *21*, 117.
- [8] B. Ruffell, L. M. Coussens, *Cancer Cell* **2015**, *27*, 462.
- [9] L. Bingle, N. J. Brown, C. E. Lewis, *J. Pathol.* **2002**, *196*, 254.
- [10] R. Ostuni, F. Kratochvill, P. J. Murray, G. Natoli, *Trends Immunol.* **2015**, *36*, 229.
- [11] P. M. Zheng, Q. Luo, W. W. Wang, J. H. Li, T. T. Wang, P. Wang, L. Chen, P. Zhang, H. Chen, Y. Liu, P. Dong, G. H. Xie, Y. H. Ma, L. Jiang, X. L. Yuan, L. S. Shen, *Cell Death Dis.* **2018**, *9*, 434.
- [12] S. C. Funes, M. Rios, E. V. Jorge, A. M. Kalergis, *Immunology* **2018**, *154*, 186.
- [13] M. Sylvestre, C. A. Crane, S. H. Pun, *Adv. Mater.* **2020**, *32*, 1902007.
- [14] X. Guo, X. Wei, Z. Chen, X. B. Zhang, G. Yang, S. B. Zhou, *Prog. Mater. Sci.* **2020**, *107*, 100599.
- [15] Q. Q. Qu, Y. Wang, L. Zhang, X. B. Zhang, S. B. Zhou, *Small* **2016**, *12*, 1378.
- [16] Y. Wang, G. Q. Wei, X. B. Zhang, X. H. Huang, J. Y. Zhao, X. Guo, S. B. Zhou, *Small* **2018**, *14*, 1702994.
- [17] Q. H. Feng, Y. Z. Li, N. Wang, Y. T. Hao, J. B. Chang, Z. Y. Wang, X. L. Zhang, Z. Z. Zhang, L. Wang, *Small* **2020**, *16*, 2002138.
- [18] M. Ovais, M. Guo, C. Chen, *Adv. Mater.* **2019**, *31*, 1808303.
- [19] L. Cassetta, J. W. Pollard, *Nat. Rev. Drug Discovery* **2018**, *17*, 887.
- [20] L. Pang, J. Qin, L. M. Han, W. J. Zhao, J. M. Liang, Z. Y. Xie, P. Yang, J. X. Wang, *Oncotarget* **2016**, *7*, 37081.
- [21] Q. Jiang, K. Wang, X. Y. Zhang, B. S. Ouyang, H. X. Liu, Z. Q. Pang, W. L. Yang, *Small* **2020**, *16*, 2001704.
- [22] J. J. Zhao, Z. K. Zhang, Y. X. Xue, G. Q. Wang, Y. Cheng, Y. C. Pan, S. L. Zhao, Y. Y. Hou, *Theranostics* **2018**, *8*, 6307.
- [23] X. Wei, L. Q. Liu, X. L. Li, Y. Wang, X. Guo, J. Y. Zhao, S. B. Zhou, *J. Controlled Release* **2019**, *313*, 42.
- [24] T. T. Wang, H. Zhang, Y. B. Han, H. H. Liu, F. Ren, J. F. Zeng, Q. Sun, Z. Li, M. Y. Gao, *ACS Appl. Mater. Interfaces* **2019**, *11*, 16367.
- [25] S. Zanganeh, G. Hutter, R. Spitler, O. Lenkov, M. Mahmoudi, A. Shaw, J. S. Pajarinen, H. Nejadnik, S. Goodman, M. Moseley, L. M. Coussens, H. E. Daldrup-Link, *Nat. Nanotechnol.* **2016**, *11*, 986.
- [26] H. J. Zhao, B. B. Zhao, L. X. Wu, H. F. Xiao, K. L. Ding, C. X. Zheng, Q. L. Song, L. L. Sun, L. Wang, Z. Z. Zhang, *ACS Nano* **2019**, *13*, 12553.
- [27] L. J. Luo, M. Z. Iqbal, C. Liu, J. Xing, O. U. Akakuru, Q. L. Fang, Z. H. Li, Y. L. Dai, A. G. Li, Y. Guan, A. G. Wu, *Biomaterials* **2019**, *223*, 119464.
- [28] F. Zhang, F. Li, G. H. Lu, W. D. Nie, L. J. Zhang, Y. L. Lv, W. E. Bao, X. Y. Gao, W. Wei, K. Y. Pu, H. Y. Xie, *ACS Nano* **2019**, *13*, 5662.
- [29] W. T. Li, B. X. Xue, K. Shi, Y. Qu, B. Y. Chu, Z. Y. Qian, *Appl. Mater. Today* **2019**, *14*, 84.
- [30] C. X. Li, Y. Zhang, X. Dong, L. Zhang, M. D. Liu, B. Li, M. K. Zhang, J. Feng, X. Z. Zhang, *Adv. Mater.* **2019**, *31*, 1807211.
- [31] Y. Zhou, K. T. Que, Z. Zhang, Z. J. Yi, P. X. Zhao, Y. You, J. P. Gong, Z. J. Liu, *Cancer Med.* **2018**, *7*, 4012.
- [32] L. Rong, Y. Zhang, W. S. Li, Z. G. Su, J. I. Fadhil, C. Zhang, *Biomaterials* **2019**, *225*, 119515.
- [33] Z. Y. Gu, T. Q. Liu, J. Tang, Y. N. Yang, H. Song, Z. K. Tuong, J. Y. Fu, C. Z. Yu, *J. Am. Chem. Soc.* **2019**, *141*, 6122.
- [34] R. G. Jin, L. Liu, W. C. Zhu, D. Y. Li, L. Yang, J. M. Duan, Z. Y. Cai, Y. Nie, Y. J. Zhang, Q. Y. Gong, B. Song, L. P. Wen, J. M. Anderson, H. Ai, *Biomaterials* **2019**, *203*, 23.
- [35] Y. W. Choo, M. Kang, H. Y. Kim, J. Han, S. Kang, J. R. Lee, G. J. Jeong, S. P. Kwon, S. Y. Song, S. Go, M. Jung, J. Hong, B. S. Kim, *ACS Nano* **2018**, *12*, 8977.

- [36] Z. M. Tang, D. Li, H. L. Sun, X. Guo, Y. Chen, S. B. Zhou, *Biomaterials* **2014**, *35*, 8015.
- [37] H. B. Hou, X. H. Huang, G. Q. Wei, F. N. Xu, Y. Wang, S. B. Zhou, *ACS Appl. Mater. Interfaces* **2019**, *11*, 29579.
- [38] J. Li, X. Zhen, Y. Lyu, Y. Jiang, J. Huang, K. Pu, *ACS Nano* **2018**, *12*, 8520.
- [39] H. Ranji-Burachaloo, P. A. Gurr, D. E. Dunstan, G. G. Qiao, *ACS Nano* **2018**, *12*, 11819.
- [40] G. Q. Wei, Y. Wang, X. H. Huang, G. Yang, J. Y. Zhao, S. B. Zhou, *J. Mater. Chem. B* **2018**, *6*, 8137.
- [41] C. R. Shi, T. Liu, Z. D. Guo, R. Q. Zhuang, X. Z. Zhang, X. Y. Chen, *Nano Lett.* **2018**, *18*, 7330.
- [42] E. M. Bachelder, T. T. Beaudette, K. E. Broaders, J. M. J. Fréchet, M. T. Albrecht, A. J. Mateczun, K. M. Ainslie, J. T. Pesce, A. M. Keane-Myers, *Mol. Pharmaceutics* **2010**, *7*, 826.
- [43] R. Klose, M. G. Adam, E. M. Weis, I. Moll, J. Wustehube-Lausch, F. Tetzlaff, C. Oka, M. Ehrmann, A. Fischer, *Oncogene* **2018**, *37*, 4260.
- [44] Y. Zhang, K. M. Cai, C. Li, Q. Guo, Q. J. Chen, X. He, L. S. Liu, Y. J. Zhang, Y. F. Lu, X. L. Chen, T. Sun, Y. Z. Huang, J. J. Cheng, C. Jiang, *Nano Lett.* **2018**, *18*, 1908.
- [45] J. Sun, S. B. Zhou, P. Hou, Y. Yang, J. Weng, X. H. Li, M. Y. Li, *J. Biomed. Mater. Res., Part A* **2007**, *80A*, 333.
- [46] Y. Gao, J. Y. Zhao, X. B. Zhang, X. Wei, X. Xiong, X. Guo, S. B. Zhou, *J. Mater. Chem. B* **2017**, *5*, 4943.